ARCHIVIO ISTITUZIONALE
DELLA RICERCA

Alma Mater Studiorum Università di Bologna
Archivio istituzionale della ricerca

Medicinal Au(I) compounds targeting urease as prospective antimicrobial agents: unveiling the structural basis for enzyme inhibition

This is the final peer-reviewed author's accepted manuscript (postprint) of the following publication:

Published Version:
Luca Mazzei, L.M. (2021). Medicinal Au(I) compounds targeting urease as prospective antimicrobial agents: unveiling the structural basis for enzyme inhibition. DALTON TRANSACTIONS, 50(40), 14444-14452 [10.1039/d1dt02488d].

Availability:
This version is available at: https://hdl.handle.net/11585/836124 since: 2021-10-25

Published:

DOI: http://doi.org/10.1039/d1dt02488d

Terms of use:

Some rights reserved. The terms and conditions for the reuse of this version of the manuscript are specified in the publishing policy. For all terms of use and more information see the publisher's website.

This item was downloaded from IRIS Università di Bologna (https://cris.unibo.it/).
When citing, please refer to the published version.

(Article begins on next page)

07 December 2025

Medicinal Au(I) compounds targeting urease as prospective antimicrobial agents: unveiling the structural basis for enzyme inhibition

Luca Mazzei[a,*] Lara Massai,[b] Michele Cianci,[c] Luigi Messori,[b] Stefano Ciurli,[a,*]

a Laboratory of Bioinorganic Chemistry, Department of Pharmacy and Biotechnology (FaBiT), University of Bologna, Via Giuseppe Fanin 40, I-40127 Bologna (Italy)
b Department of Chemistry “Ugo Schiff”, University of Florence, Via della Lastruccia 3-13, I-50019 Sesto Fiorentino (Italy)
c Department of Agricultural, Food and Environmental Sciences, Polytechnic University of Marche, Via Brecce Bianche, I-60131 Ancona (Italy)

Luca Mazzei: ORCID 0000-0003-1335-9365
Lara Massai: ORCID 0000-0003-0765-1802
Michele Cianci: ORCID 0000-0001-5607-6061
Luigi Messori: ORCID 0000-0002-9490-8014
Stefano Ciurli: ORCID 0000-0001-9557-926X

Keywords: Nickel; urease; X-ray crystal structure; gold; phosphine; enzyme inhibition

* Corresponding authors: luca.mazzei2@unibo.it, stefano.ciurli@unibo.it

ABSTRACT

A few gold compounds were recently found to show antimicrobial properties in vitro, holding great promise for the discovery of new drugs to overcome antibiotic resistance. Here, the inhibition of the bac- terial virulence factor urease by four Au(I)-compounds, namely $Au(PEt_3)Cl$, $Au(PEt_3)Br$, $Au(PEt_3)I$ and $[Au(PEt_3)_2]Cl$, obtained from the antiarthritic Au(I)-drug Auranofin and earlier reported to act as antimicro- bials, is investigated. The three monophosphino Au(I) complexes showed IC50 values in the 30–100 nM range, while the diphosphino Au(I) complex, though being less active, still showed a IC_{50} value of 7 μM. The structural basis for this inhibition was provided by solving the crystal structures of urease co-crystal- lized with $Au(PEt_3)I$ and $[Au(PEt_3)_2]Cl$: at least two Au(I) ions bind the enzyme in a flap domain involved in the catalysis, thus obliterating enzyme activity. Peculiar changes observed in the two structures reveal implications for the mechanism of soft metal binding and enzyme inactivation.

INTRODUCTION

Medicinal metal compounds form a promising, structurally varied and still largely unexplored class of chemical sub- stances with great potential for the discovery of new therapeutics.[1] Indeed, medicinal metal compounds bear a variety of metal centres such as Cu, Fe, Au, Pt, Pd, or Bi, with unique reactivity properties toward biomolecules that may well result in the innovative mechanisms of action and un- precedented pharmacological activities, while at the same time decreasing the toxicity of bare metal ions.[1] Much atten- tion has recently been focused on gold compounds as prospective antibacterial agents in relation to the so called “antibiotic crisis” and to the rapid emergence of several multi- resistant pathogens.[2] In particular, several gold compounds are being developed as therapeutic agents for human diseases to become versatile and powerful drugs for diseases caused by the dysfunction of selenol and thiol containing proteins.[3] Within this frame, the clinically established gold(I) drug Auranofin (Scheme 1) is playing a pivotal role as a leading antimicrobial agent.[4]

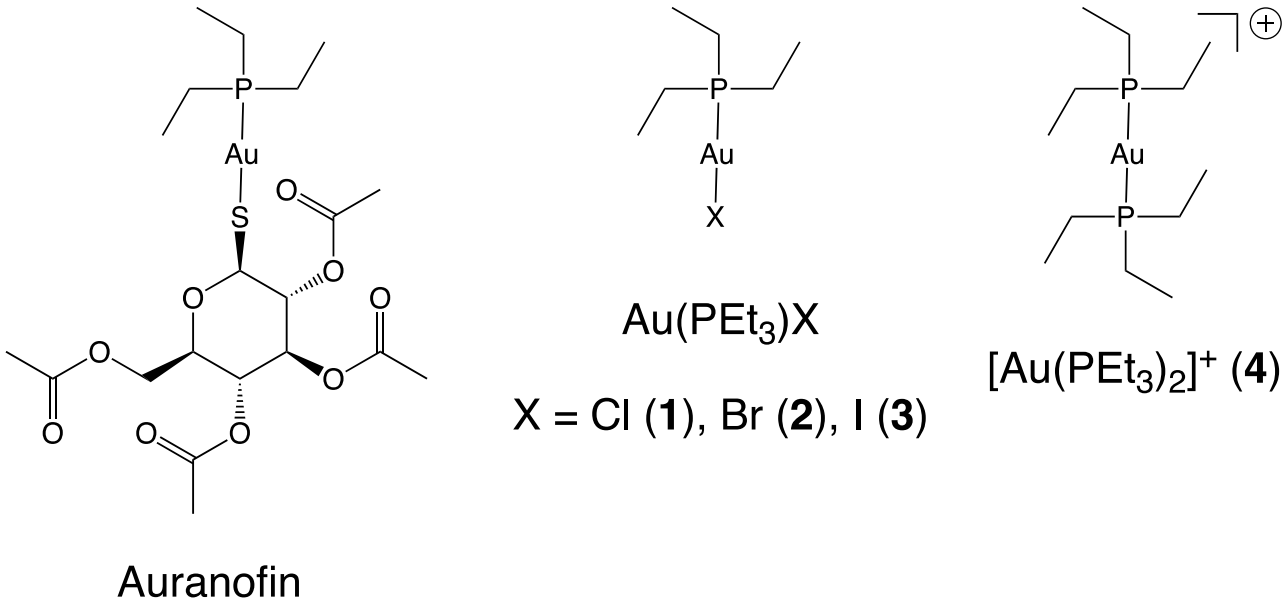

Scheme 1. Structure of Auranofin and the Au(I) complexes considered in the present study.

Indeed, Auranofin was recently reported to exhibit significant antibacterial properties against a variety of Gram-positive and a few Gram-negative bacteria.[5] Some initial mechanistic studies were carried out as well, and demonstrated that Auranofin's antibacterial activity features a complex process that may involve the inhibition of multiple biosynthetic path- ways including cell wall, DNA, and bacterial protein synthesis.[6] More in general, these findings increased the interest of scientists toward gold compounds as a rich source of new antibacterial drug candidates. Recently, some of us published a study where the antibacterial properties of Auranofin and a panel of its Au(I) and Ag(I) derivatives were assayed in vitro towards several pathogens, including a few multi-resistant strains, with encouraging results.[7] Among these, Au(I) compounds inhibited the bacterial growth of Gram-positive strains with minimal inhibitory concentration (MIC) values in the range of 1–65 μM. Generally, the diphosphino Au(I) complex turned out to be less effective than the mixed phosphino halido Au(I) complexes probably as a consequence of the fact that the phosphine ligand is a worse leaving group compared to halides.[7]

Urease (urea amidohydrolase, E.C. 3.5.1.5) is a nickel dependent enzyme that is largely distributed among plants, fungi, and bacteria. Urease is a very efficient hydrolase that accelerates the rate of urea hydrolysis (Scheme 2) by about one-hundred-trillion-times.[8]

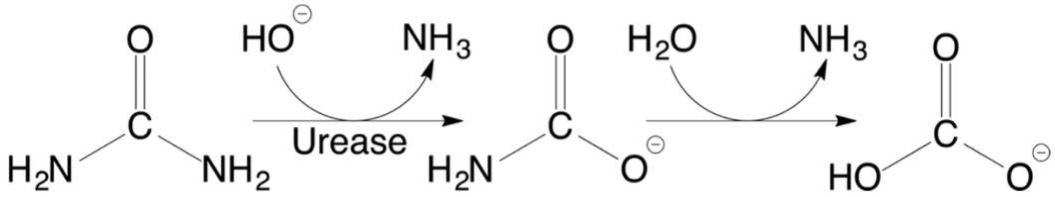

Scheme 2. Hydrolysis of urea catalysed by urease

The increase of the pH of the medium brought about by urease through the production of ammonia is a strategy of great medical concern.[9] Indeed, urinary and/or gastrointestinal infections caused by ureolytic bacteria may increase the pH value appreciably and give rise to severe complications such as kidney stone formation, pyelonephritis, hepatic encephalopathy, and hepatic coma;[10] *Helicobacter pylori* containing a large amount of urease represents the best-known example of this kind of pathogen,[11] together with *Staphylococcus aureus*,[12] *Mycobacterium tuberculosis*,[13] as well as *Proteus mirabilis*, *Staphylococcus saprophyticus* and by a few strains of *Escherichia coli*.[14] Owing to their crucial role in bacterial survival, ureases have become important therapeutic targets for the treatment of diseases caused by urease-dependent pathogenic microorganisms.

Several reports now suggest that urease is a relevant target for metal compounds.[15] Indeed, a variety of metal species and metal complexes were reported to bind the enzyme tightly and to induce a strong inhibition of its catalytic activity. The inhibitory efficacy of heavy metal ions on the activity of urease has been extensively documented for the enzyme from *Canavalia ensiformis*; various metal ions were ordered according to their inhibition potency, as Hg(II) ≈ Ag(I) > Cu(II) ≫ Ni(II) > Cd(II) > Zn(II) > Co(II) > Fe(III) > Pb(II) > Mn(II).[16] The structural basis for the binding of some Ag(I) and Au(III) compounds to urease was recently elucidated;[17] in the latter case, metal binding to urease requires a reduction step from Au(III) to Au(I).

Based on these observations, four Au(I) analogues of Auranofin, in which the thio-sugar ligand is replaced with chloride, bromide or iodide in $Au(PEt_3)Cl$ (**1**), $Au(PEt_3)Br$ (**2**), and $Au(PEt_3)I$ (**3**), or with a second phosphine ligand, as in the case of $[Au(PEt_3)_2]Cl$ (**4**) (Scheme 1), were investigated and found to be effective inhibitors of *Canavalia ensiformis* (jack bean) urease (JBU). The molecular basis of this inhibition was further investigated using X-ray crystallography: the structures of the bacterial urease from *Sporosarcina*

pasteurii (SPU), largely homologous to JBU and used in the past two decades as a model enzyme to study structure–function relationships in ureases because of its well-established crystallization conditions, revealed the location of Au(I)-binding sites on the protein and consequently indicated the main determinants of enzyme inhibition. The knowledge gained from the present study may turn valuable for the design and synthesis of novel Au-based compounds with more selective and/or improved antimicrobial properties.

MATERIALS AND METHODS

Preparation of the enzymes

Sporosarcina pasteurii urease (SPU) (molecular mass = 250 kDa) was obtained in a pure form from *Sporosarcina pasteurii* DSM 33 bacterial cells following a previously reported expression and purification procedure18 and stored at +4 °C. JBU (molecular mass = 550 kDa) type C-3 (powder, ≥600 000 units per g solid) was purchased from Sigma-Aldrich, dissolved in 20 mM HEPES buffer, at pH 7.5, and stored at −80 °C as stock aliquots. Enzyme quantification was carried out by measuring the activities of SPU and JBU at pH 7.0 through a pH-STAT method,[19] considering their specific activities of 2500 and 3500 units per mg,[16c] respectively.

Preparation of the Au(I) complexes

Starting from the commercially available Auranofin analogue **1** in which the thio-sugar ligand is replaced with one chloride ligand, the bromide and iodide Auranofin analogues **2** and **3** were synthesized as previously described.[7] The diphosphino derivative of Auranofin **4** was also synthesized starting from 1 according to literature data.[7] Stock solutions of 1–3 (100 mM) and 4 (80 mM) were prepared by dissolving the corresponding powders in dimethyl sulfoxide (DMSO).

Inhibition assays

The characterization of urease inhibition by compounds **1**–**4** was performed on JBU at room temperature following a published procedure.[20] A 10 mM HEPES buffer at pH 7.5, also containing 10 % (v/v) DMSO, was used to dilute the stock solutions of the Au(I) compounds to a final concentration of 100 μM in the cases of **1**–**3**, or 1 mM for **4**. Reaction mixtures (1 mL) were prepared by adding (i) 1 nM of active JBU and (ii) increasing concentrations of each Au(I) compound (in the range of 1.0–400 nM for **1**–**3**, and in the range of 0.1–100 μM for **4**) to a 30 mg L^{-1} cresol red solution prepared in 2 mM HEPES buffer, at pH 7.5, and treated with CHELEX® resin (Sigma-Aldrich) prior to enzyme addition to remove any metal ions possibly interfering with JBU activity. After a one-hour incubation, the experiment was started by the addition of 100 mM urea and following the overtime change in absorbance at 573 nm, due to the change in the colour of cresol red upon the pH increase consequent to urease activity, by using an Agilent Cary 60 UV– Vis spectrophotometer. The JBU reaction rates at each concentration of **1**–**4** (v_i), calculated as the slope of the straight portion of the absorbance *vs*. time curve, were normalized with respect to the JBU reaction rate measured in the absence of **1**–**4** (v_0) to obtain residual activity values (%) (all experiments were performed in triplicate). The resulting data were plotted as a function of concentration and fitted using the Prism v. 8.4.3 software, to estimate the values of concentration of **1**–**4** that induced 50 % inhibition of JBU (IC_{50}).

Crystallization trials

Working solutions of 12 mM **1**–**3** and 25 mM **4** were prepared by dissolving the corresponding stock solutions in 50 mM HEPES buffer at pH 7.5, also containing 50 mM Na_2SO_3. A 10 % volume of each working solution was added to an aliquot of 11 mg mL^{-1} SPU dissolved in 50 mM HEPES buffer, at pH 7.5, also containing 50 mM Na_2SO_3 as a

preservative, obtaining SPU – ligand incubation mixtures at a final concentration of 0.6 mM for **1** and **2**, 1.2 mM for **3**, and 2.5 mM for **4**. After an appropriate incubation time necessary to obliterate the enzyme activity (approximately 2–3 hours), crystallization drops were plated by diluting 1.5 µL of each SPU–Au(I) compound solution with 1.5 µL of a precipitant solution containing 1.2–1.7 M $(NH_4)_2SO_4$ and the same concentration of the Au(I) compound as that present in the incubation mixture.

Crystallization trials were performed at 293 K using the vapor diffusion technique (the hanging-drop method), equilibrating the drop against 1 mL of the precipitant solution (in the absence of the ligand in the reservoir) using 24-well XRL Plates (Molecular Dimensions). Rice-shaped protein crystals (dimensions up to 0.07 × 0.07 × 0.2 mm^3) of SPU incubated with **2**–**4** grew in the presence of 1.3–1.6 M $(NH_4)_2SO_4$ after two weeks. No crystals were obtained in the case of **1**, while further crystallization trials using lower concentrations of this derivative also failed. Cryoprotection was ensured by transferring the crystals to a solution containing 1.8 M $(NH_4)_2SO_4$ and 20 % (v/v) ethylene glycol, also added to 2.5 mM of the corresponding Au(I) compound, and then flash-cooled and stored in liquid nitrogen.

X-ray diffraction data collection and structural determination

X-ray diffraction data collection was carried out at the EMBL P13 beamline of the Petra III storage ring, c/o DESY, Hamburg (Germany).[21] Data were collected at 100 K by performing helical scans to achieve higher data quality by minimizing radiation damage. Data processing and reduction were carried out using XDS[22] and AIMLESS.[23] The crystals were highly isomorphic to those of all previous reported SPU crystals and belonged to the space group $P6_322$.

Structural determination was carried out by restrained refinement using REFMAC5.[24] Initial phases were obtained from the X-ray crystal structure of SPU inhibited in the presence of NBPT and found in the complex with MATP (PDB code 5OL4), determined at 1.28 Å.[25] The phasing model, devoid of residues 311–340 of the α subunit, namely the amino acid portion forming the mobile flap region, and of any other non-proteinaceous ligands except for the active site Ni(II) ions, was subjected to coordinate randomization in order to remove any potential phase bias. Refinement was conducted using isotropic atomic displacement parameters (ADPs) for proteinaceous and Ni atoms (including the addition of the hydrogen atoms in the riding positions) and anisotropic ADPs for Au atoms and their non-proteinaceous ligands, to improve residual density maps by considering the possible vibrational components of Au adducts.[26] Manual model rebuilding, including water and ligand addition/inspection, was carried out using COOT.[27] The unbiased omit electron density maps were calculated with Fourier coefficients $F_o - F_c$ and phases from the last cycle of refinement before ligand addition.

Model coordinates and structural factors of the X-ray crystal structures of SPU co-crystallized in the presence of compounds **3** and **4** were deposited in the Protein Data Bank (PDB) under the accession codes 7P7N and 7P7O, respectively. Data collection, processing and final refinement statistics are given in Table 1-ESI. The figures were generated using PyMol (The PyMOL Molecular Graphics System, v. 1.8 Schrödinger, LLC), and CrystalMaker v. 10.6.2 (http://www.crystalmaker.com).

DFT calculations

The ground state equilibrium geometry of the compounds of general formula $M(PEt_3)X$, where M = Ag(I) or Au(I), and X = Cl, Br, I, or PEt_3, in the gas phase, was determined using quantum-chemical Density Functional Theory (DFT) calculations with the ωB97X-D functional and the 6-31G* basis set, implemented in the commercially available Spartan'20 software (Wavefunction, Inc.).

RESULTS AND DISCUSSION

Urease inhibition profiles by gold complexes and associated structure–function relationships

Urease inhibition by compounds **1**–**4** was characterized by measuring the enzymatic activity of JBU in the presence of 100 mM urea and increasing concentrations of each Au(I) compound, and then estimating the corresponding IC_{50} values (Fig. 1). The results (plotted on a semi-log graph) show characteristic sigmoidal profiles reaching in all cases full enzyme inactivation: the mono-phosphino neutral complexes **1**–**3** show IC_{50} values in the nanomolar range that increases in the order **3** < **2** < **1**, while the IC_{50} value for the diphosphino cationic complex **4** falls in the low-micromolar range, with an increase of two orders of magnitude with respect to the values found for the mono-phosphino compounds.

Overall, the inhibition strengths of mono-phosphino compounds **1**–**3** on JBU are comparable to those observed on the same enzyme for a series of coordination and organometallic Au(III) compounds recently characterized as urease inhibitors,[17b] confirming the very high affinity of the gold compounds for urease. Moreover, the IC_{50} values of compounds **1**–**3** fall in the same nanomolar range as that reported for structurally related mixed phosphino/halido Ag(I) compounds, also following the same order of inhibition efficacy.[20] In the latter case, these observations were interpreted as suggesting a step of Ag(I) ligand substitution by an enzyme functional group that is essential for catalysis.[20] While in the case of the ionic diphosphino complex the initial ligand substitution must necessarily involve one of the two PEt_3 ligands; for the mixed ligand complexes Et_3P–M–X (M = Ag or Au) the question arises as to which ligand, namely the phosphine or the halide, is initially substituted by the enzyme functional group. Based on the available metal–ligand distances for the series of $Ag(PEt_3)X$ complexes (Table 1),[28] and considering both the absence of any residual halide or phosphine ligand on the Ag–SPU complex determined by crystallography and the significantly decreased urease inhibition efficiency of the diphosphino adduct, it was suggested that, in the case of the Ag(I) complexes, the initial leaving group is the PEt_3 ligand.[20] In the case of analogous Au(I) compounds **1**–**4** considered in the present study, only the crystal structure of $Au(PEt_3)Cl$ (**1**) has been reported (Table 1),[29] making it impossible to build a rationale based on known metal-ligand distances as done in the Ag(I) case. With the aim to compare the structural properties of compounds **1**–**4**, DFT calculations were thus carried out. The results indicate that, also in the case of the Au(I) analogues, the Au–X distance significantly increases in the order Au–Cl < Au–Br < Au–I, while the Au–P distance is relatively less affected by the identity of the bound halide (Table 1). Therefore, a rationale can be developed to support either (i) the hypothesis of the halide being firstly substituted (because of the increasing leaving group character and the M–X distance in the sequence Cl < Br < I) or (ii) the phosphine being replaced first (due to the increasingly weakening of the M–P bond in the sequence Cl < Br < I); in both cases, the trend would be consistent with that of the IC_{50} values determined for compounds **1**–**3**. This issue was further investigated following the structural determination of the complexes formed after the inactivation of urease by compounds **1**–**4**. As discussed below, the presence of a residual phosphino ligand bound to the Au(I) atoms in the SPU adducts resulting from the inactivation of urease with mixed phosphino/halido complexes, together with the absence of any residual halide ion, is a strong indication that the initial leaving group is the halide, clarifying early questions and reports.[20]

General structural features of inactivated urease

Crystallization trials of SPU were carried out in the presence of **1**–**4**, yielding single crystals only for **2**–**4**, which were used for X-ray diffraction data collection. The analysis carried out on the structure of SPU co-crystallized in the presence of the bromide derivative **2** revealed the absence of any modification of the native protein, and no further

analysis was carried out. On the other hand, in the case of SPU co-crystallized in the presence of **3** and **4**, while the overall analysis of the active site of the structures showed a Ni-coordination framework completely conserved with respect to that of the native enzyme30 (Table 2-ESI), significant changes were detected and ascribed to alterations induced by the interaction of the enzyme with the tested gold compounds, leading to its inactivation.

The α, β and γ subunits, which involve the crystallographic asymmetric units of the two X-ray crystal structures and form the characteristic $(\alpha\beta\gamma)_3$ quaternary assembly of SPU, display backbone conformations very similar to that of the native enzyme (PDB code 4CEU), as revealed by the per residue Cα RMSD analysis (Fig. 1-ESI). However, two regions exhibiting higher RMSD values are detectable in the α subunit at the level of (i) the so-called mobile flap (comprising residues α311–α340) that modulates the active site channel opening and closing, allowing substrate access and product release[8d,e,31] and (ii) the solvent-exposed C-terminal portion of the α subunit (residues α540-α560).

In general, the mobile flap regions of the two X-ray crystal structures are highly disordered. Poor and hardly interpretable portions of the electron density maps in those regions prevented residues α324-α329 and α331-α337 to be modelled for the structures of SPU crystallized in the presence of **3** and **4**, respectively. In particular, the flap region of the structure of SPU crystallized in the presence of **4** shows relatively high RMSD values with respect to native SPU for residues α325-α330 (up to ca. 12 Å for residues αGln327 and αAsn328). In both cases, significant shifts of ca. 3 Å and 4 Å are observed for the Cα atoms of the αCys322 and αHis323 residues that are critical for the urease enzymatic catalysis.[8d] In turn, a movement of ca. 5 Å of the αCys322 Sγ atom, together with a ca. 10 Å shift in the position of the imidazole ring of αHis323, are observed, the large value for the latter being most likely due to a rotation by ca. 180° of the αHis323 side chain from pointing towards the active site cavity to pointing it towards the bulk solvent.

The solvent-exposed regions at the C-terminus of the α subunit are less affected than the mobile flap by interaction of SPU with **3** and **4**, with the highest RMSD value involving αAsp549 (ca. 2 Å), a residue located on a short turn that com- prises six residues upstream of the solvent exposed αCys555. The side chain of the latter residue is rotated from pointing its Sγ atom towards the protein core to pointing it towards the bulk solvent.

The unbiased omit electron density maps of the structures of SPU inactivated by **3** revealed four strong positive peaks indicating the presence of non-proteinaceous heavy atoms, located in conserved positions: three peaks were found close to the active site mobile flap region and in particular close to the side chains of αCys322 and αMet367 (Fig. 2A), the latter residue being located on a rigid portion of the active site and facing the flap; a fourth peak was detected near the solvent-exposed C-terminal portion of the α subunit, in the vicinity of the side chain of αCys555 (Fig. 2B). The anomalous electron density maps indicated unarguably the presence of Au(I) atoms in all those four positions (Fig. 2A and B).

The three positive electron density peaks in the active site were successfully examined and refined using three Au(I) ions (Fig. 2C and 4A). In particular, Au(1) and Au(2) (both with occupancies of 50 %) are bridged by the αCys322 Sγ thiolate (Au–S distance = 2.8 and 2.7 Å). No additional electron density was detected around Au(1) and Au(2), with the expected linear coordination geometry being conceivably completed by the presence of disordered, and therefore not visible, water molecules. On the other hand, Au(3) (with an occupancy of 35 %) is bound to the thioether αMet367 Sδ atom (Au–S distance = 2.7 Å) and to the O atom of an additional, and detectable (Fig. 2A), electron density modelled as a water molecule (O_W) that completes a linear coordination geometry (Au–O distance = 2.7 Å) (Fig. 2C and 4A). Finally, the electron density near αCys555 was modelled using a gold atom, Au(4), linearly brid- ging the cysteine side chain thiolate (Au–S distance = 2.5 Å) and a residual PEt_3 ligand (Au–P distance = 2.3 Å) making up the so-called AUF moiety (with

an occupancy of 80 %, Fig. 2D and 4B). A complete list of distances and angles around the Au atoms is reported in Table 2.

The unbiased omit electron density maps of the structures of SPU inactivated by **4** revealed instead only two strong positive peaks located close to the active site in the same positions as in the previous case, with the peak close to the side chain of αMet367 missing (Fig. 3A); a third peak was detected in the vicinity of the side chain of αCys555 (Fig. 3B). Also in this case, the anomalous electron density maps indicated unarguably the presence of Au(I) atoms in all these three cases. Attempts to model only two single Au(1) and Au(2) atoms in these positions did not yield a satisfactory refinement because additional electron density was detectable close to each metal ion (Fig. 3A). A successful modelling of this density was instead achieved by including two PEt_3 ligands (making up two AUF moieties, with occupancies of 70 %) (Fig. 3B and 4C) completing a linear coordination geometry around each Au(I) atom (Au–P distances of 2.7 and 2.5 Å). The presence of a gold atom, linearly bound to αCys555 Sγ and to a PEt_3 ligand (making up an AUF moiety with an occupancy of 80 %) was also observed as in the previous case (Fig. 4D).

For both crystal structures, the short Au···Au distance (ca. 3.2 Å), the small Au–αCys322 Sγ–Au angle (ca. 74°) and the slight distortion of the Et_3P–Au–αCys322 Sγ angle (ca. 170°), caused by a bowing effect of the two Au atoms towards each other, support the presence of a weak metal–metal bond between the two Au(I) ions similar to what observed for both Au(I)[17b,32] and Ag(I)[17a,20] binuclear clusters.

The two X-ray crystal structures determined in the present study were compared with the recently reported X-ray crystal structure of SPU co-crystallized in the presence of the Au(III) compound $[Au(PbImMe)Cl_2]PF_6$ (PbImMe = 1-methyl-2- (pyridin-2-yl)-benzimidazole) (**5**) and featuring bound Au(I) atoms resulting from a two-electron reduction of the starting inhibitor (PDB code 6I9Y).[33] In all cases a binuclear Au(I) cluster is formed in the active site cavity, bridged by the αCys322 Sγ atom; however, each Au(I) ion completes a linear coordination geometry by binding αHis323 Nδ and αMet367 Sδ in the case of SPU inactivated by **5**,[33] while either solvent molecules or residual tri-ethyl phosphine ligands make up a linear coordination in the case of SPU inactivated by **3** or **4**. Moreover, while a gold(I) atom was observed to be bound to αMet367 Sδ in the case of SPU inactivated by **3**, no additional metal ions were found in this position in the case of SPU inactivated by **5**. Finally, the presence of an Au(I) ion coordinated to αCys555 Sγ was observed in all cases of SPU inactivated by either **5**[33] (presumably bound to disordered water molecules) or **3** and **4** (bound to a residual PEt_3 ligand), and this can therefore be considered a conserved feature that highlights the reactivity of this solvent-exposed cysteine residue vs. gold compounds. The per residue Cα RMSD analysis performed on the present X-ray structures with respect to SPU inactivated by **5** (Fig. 2-ESI) shows comparable backbone displacements of the active site flap region with respect to the native enzyme, and smaller modifications for the C-terminal region. However, while the mobile flap region of SPU inactivated by **5** is rigid and only moderately deviating from that of the native enzyme except for the side chains of the Au(I)-binding residues, in the case of SPU inactivated by **3** and **4** the disorder of this motif is significantly larger and further extended to the second helix of the helix-turn-helix motif. This feature can be ascribed to the peculiar nature of the Au(I) adduct formation in this latter case, which induces an unwinding in the middle portion of the flap, thus resulting in the increase of the disorder in the portion downstream. This analysis suggests that the backbone and side chain conformations of SPU are differently affected by the distinctive binding modes of the Au(I) ions. The observation of two additional Au(I) ions at the tip of the helix-turn-helix mobile flap in the structure of SPU crystallized in the presence of **3** suggests that the residues in this region, modulating the entrance of the active site cavity, could act as ligands in the first steps of the interaction between these gold-based drugs and urease. It could thus be envisioned that this observation represents a snapshot depicting the early stages of the

Au(I) ion pathway from the bulk solvent into the active site cavity, suggesting how these metal ions could be first captured and eventually carried to their final positions. In this scenario, the Au(I) ions bound to αCys322 and αMet367 in the structures of SPU inactivated by **3** and **4** could represent a transient state that evolves, after a rearrangement and a stabilization of the mobile flap region, to a final inactivation mode as reported for the structure of SPU inhibited by **5**.

The presence of a protein-bound triethyl-phosphine Au(I) moiety, which characterizes the structures of SPU inactivated by **3** and **4**, has been reported only in three cases: (i) the peptidyl-prolyl cis–trans isomerase 3 (Cyclophilin-3) from *Caenorhabditis elegans*[34] (PDB code 1E3B) and (ii) the phosphatidylethanolamine transferase (MCR-1-S) from *Escherichia coli*[35] (PDB code 6LI6), both treated with [Au(PEt_3)Cl], and (iii) the nucleosome core particle containing the adducts of triethyl-phosphine Au(I) and ruthenium(II)-toluene PTA complexes[36] (PDB code 5DNN). In all these cases, the triethyl-phosphine Au(I) moiety was found to be ligated to the Nε atom of a histidine imidazole ring. A few other X-ray crystal protein structures determined upon crystallization in the presence of Auranofin or its analogues (PDB codes 2YAU,[37] 6LHE,[35] 4LFP,[38] 4CBQ,[39] 4CCR,[39] and 3H4K[40]) show the pres- ence of Au(I) ions coordinated by cysteine and histidine resi- dues, as well as chloride ions and water molecules. Therefore, the existence of a triethyl-phosphine Au(I) moiety bound to a thiolate cysteine Sγ atom, as reported here, is unprecedented.

CONCLUSIONS

In the search for novel metal-based agents capable of fighting multi-resistant pathogens, four gold compounds modelled on the structure of Auranofin, with known antibacterial properties, were evaluated as possible inhibitors of the enzyme urease, a recognized critical target for the development of new antimicrobials. Notably, three of these Au(I) compounds, *i.e.* the mixed phosphino/halido Au(I) complexes Au(PEt_3)Cl (**1**), Au(PEt_3)Br (**2**) and Au(PEt_3)I, (**3**) exhibited excellent i*n vitro* inhibiting properties against plant urease with IC_{50} values in the nanomolar range, while the diphosphino Au(I) complex [Au(PEt_3)$_2$]Cl (**4**) showed a weaker, though still significant, enzyme inhibition activity. For two of these Au(I) compounds, i.e. Au(PEt_3)I and [Au(PEt_3)$_2$]Cl, the crystal structures of their adducts with bacterial urease were obtained. The structures revealed that the coordination environment of the two essential Ni(II) ions in the active site is not affected at all, while at least two Au(I) ions make up a bimetallic cluster located in a protein region which modulates the active site opening, blocking its critical conformational flexibility and thus irreversibly inactivating the enzyme. This study provides the structural basis to rationalize the strong urease inactivation by metal centres with a large soft Lewis character, offering hints towards the development of new metal-based antimicrobial drugs targeting antibiotic resistant ureolytic pathogenic bacteria.

CONFLICTS OF INTEREST

There are no conflicts to declare.

ACKNOWLEDGEMENTS

This research was supported by CIRMMP (Consorzio Interuniversitario di Risonanze Magnetiche di Metallo Proteine), and by CIRCMSB (Consorzio Interuniversitario di Ricerca in Chimica dei Metalli nei Sistemi Biologici). X-ray diffraction data were collected at the PETRA III storage ring operated by EMBL Hamburg (DESY, Hamburg, Germany; beam time award number MX-720). We are thankful for the facility for the beam time and the technical support.

Table 1. Crystallographic and DFT-calculated M-L distances in $M(PEt_3)X$ complexes (M = Ag or Au); X = Cl, Br, I, PEt_3

Metal complex	M – X distance (Å)		M – PEt_3 distance (Å)	
	DFT	**X-ray**	**DFT**	**X-ray**
$Ag(PEt_3)Cl$	2.346	2.300 [28a]	2.395	2.390 [28a]
$Ag(PEt_3)Br$	2.466	2.422 [28a]	2.406	2.402 [28a]
$Ag(PEt_3)I$	2.631	2.918 [28b]	2.415	2.438 [28b]
$Ag(PEt_3)_2^+$	2.444		2.444	
$Au(PEt_3)Cl$	2.336	2.305 [29]	2.285	2.232 [29]
$Au(PEt_3)Br$	2.435		2.293	
$Au(PEt_3)I$	2.615		2.307	
$Au(PEt_3)_2^+$	2.368		2.368	

Table 2. Selected distances (Å) and angles (°) around the Au(I) ions in the crystal structures of SPU co-crystallized in the presence of $Au(PEt_3)I$ (PDB code 7P7N) and $Au(PEt_3)_2Cl$ (PDB code 7P7O).

Distances (Å)	**$Au(PEt_3)I$**	**$Au(PEt_3)_2Cl$**
Au(1) – αCys322 Sγ	2.7	2.7
Au(2) – αCys322 Sγ	2.8	2.5
Au(1) – PEt_3		2.3
Au(2) – PEt_3		2.4
Au(3) – αMet367 Sδ	2.7	
Au(3) – O_W	2.7	
Au(1) ••• Au(2)	3.2	3.2
Au(4) – αCys555 Sγ	2.5	2.2
Au(4) – PEt_3	2.3	2.3
Angles (°)		
Au(1) - αCys322 Sγ – Au(2)	72	76
Et_3P - Au(1) – αCys322 Sγ		169.9
Et_3P - Au(2) – αCys322 Sγ		171.7
αMet367 Sδ – Au(3) – O_W	171.4	
Et_3P – Au(4) – αCys555 Sγ	176.0	174.0

Figure 1. Dose – response semi-log plot for the residual activity of JBU as a function of Au(I) compounds concentration. Experimental data and corresponding non-linear data fitting are shown as dots and lines, respectively. IC_{50} values (nM) for each Au(I) compound tested is also reported.

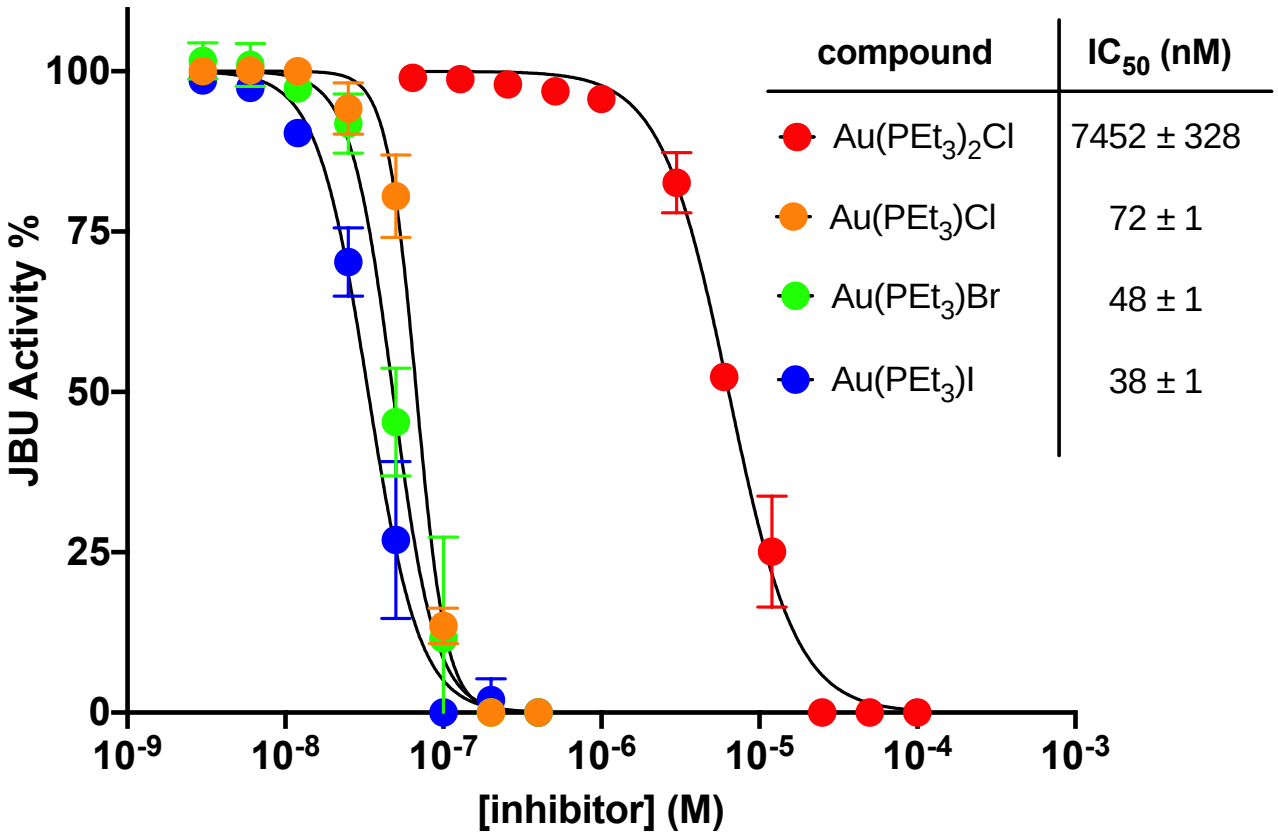

Figure 2. X-ray crystal structure of SPU co-crystallized in the presence of $Au(PEt_3)I$ (**3**). The protein atomic models, as well as the nickel ions and the active site solvent molecules, are shown superimposed onto the final $2F_o$ - F_c electron density map, contoured at 1σ and coloured grey. In panels **A** and **B** the unbiased F_o - F_c omit and the anomalous electron density maps for the ligands are shown contoured at 3σ and coloured orange and blue, respectively. In panels **C** and **D**, the modelled ligands are presented superimposed onto the final $2F_o$ - F_c electron density map, contoured at 1σ and coloured grey. Carbon, nitrogen, phosphorous, oxygen, sulphur, and nickel are grey, blue, orange, red, yellow, and green, respectively.

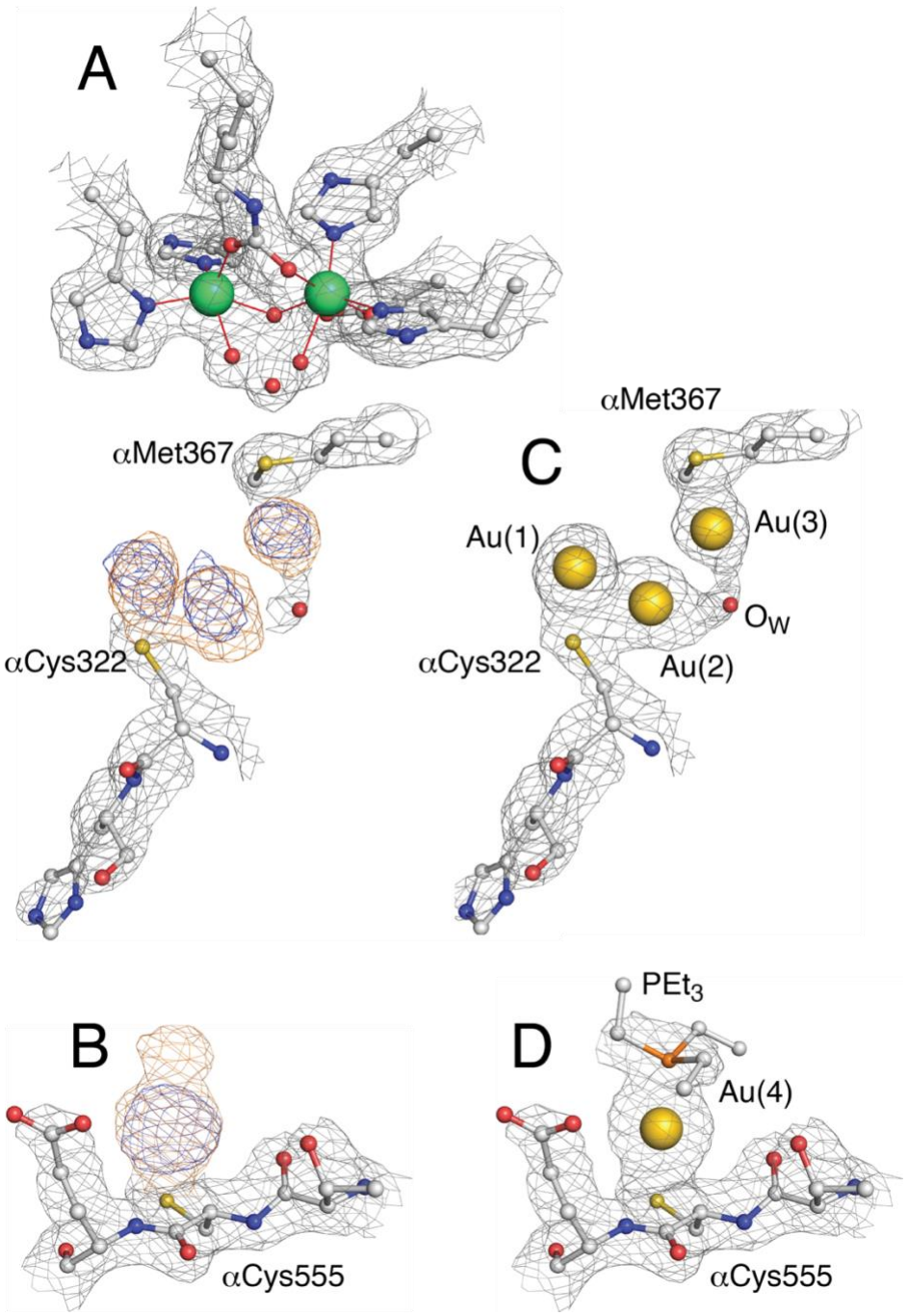

Figure 3. X-ray crystal structure of SPU co-crystallized in the presence of $Au(PEt_3)_2Cl$ (**4**). The protein atomic models, as well as the nickel ions and the active site solvent molecules, are shown superimposed onto the final $2F_o - F_c$ electron density map, contoured at 1σ and coloured grey. In panel **A** the unbiased $F_o - F_c$ omit and the anomalous electron density maps for the ligands are shown contoured at 3σ and coloured orange and blue, respectively. In panel **B** the modelled ligands are presented superimposed onto the final $2F_o - F_c$ electron density map, contoured at 1σ and coloured grey. Carbon, nitrogen, phosphorous, oxygen, sulphur, and nickel are grey, blue, orange, red, yellow, and green, respectively.

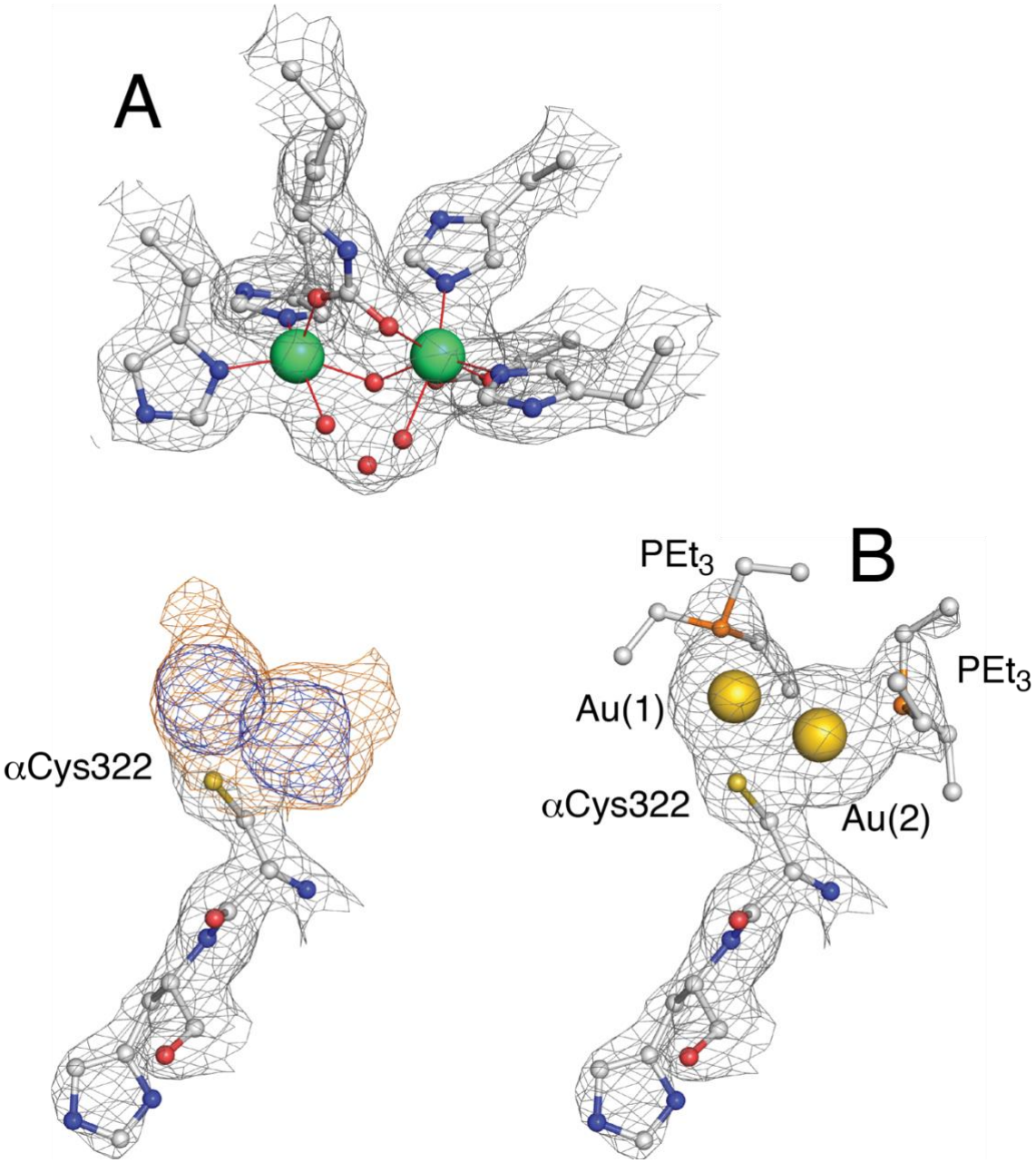

Figure 4. Structural models of the coordination environments of the Au(I) atoms determined for SPU co-crystallized in the presence of $Au(PEt_3)I$ (**3**) and $Au(PEt_3)_2Cl$ (**4**).

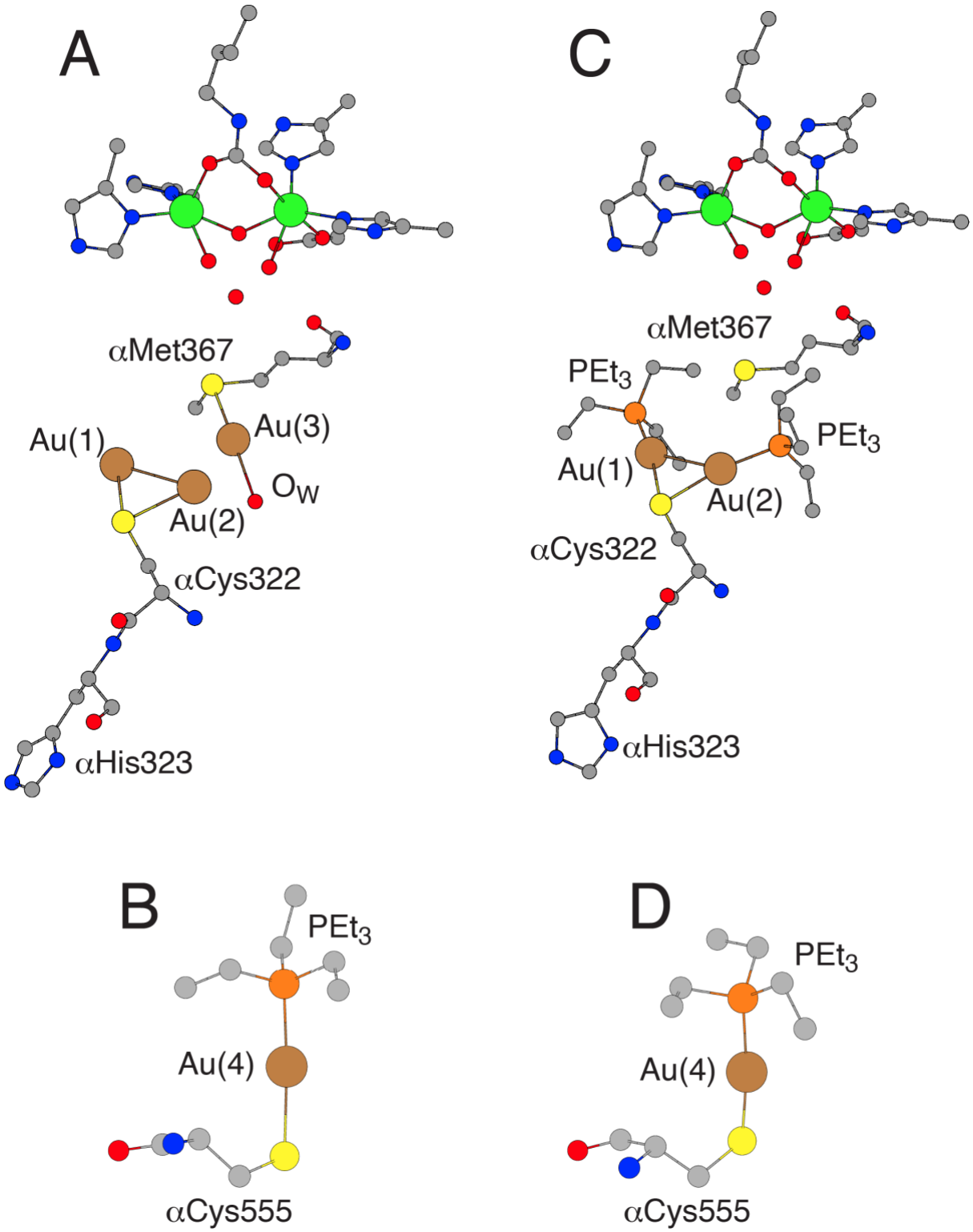

REFERENCES

[1] J. Karges, R. W. Stokes and S. M. Cohen, Trends Chem., 2021, 3, 523–534.
[2] (a) B. Wu, X. Yang and M. Yan, J. Med. Chem., 2019, 62, 7751–7768; (b) P. I. da Silva Maia, V. M. Deflon and U. Abram, Future Med. Chem., 2014, 6, 1515–1536; (c) M. J. S. A. Silva, P. M. P. Gois and G. Gasser, ChemBioChem, 2021, 22, 1740–1742.
[3] S. J. Berners-Price and A. Filipovska, Metallomics, 2011, 3, 863–873.
[4] (a) J. M. Madeira, D. L. Gibson, W. F. Kean and A. Klegeris, Inflammopharmacology, 2012, 20, 297–306; (b) M. I. Cassetta, T. Marzo, S. Fallani, A. Novelli and L. Messori, BioMetals, 2014, 27, 787–791.
[5] S. Thangamani, H. Mohammad, M. F. Abushahba, T. J. Sobreira, V. E. Hedrick, L. N. Paul and M. N. Seleem, Sci. Rep., 2016, 6, 22571.
[6] L. Felix, E. Mylonakis and B. B. Fuchs, Front. Microbiol., 2021, 12, 663481.
[7] T. Marzo, D. Cirri, S. Pollini, M. Prato, S. Fallani, M. I. Cassetta, A. Novelli, G. M. Rossolini and L. Messori, ChemMedChem, 2018, 13, 2448–2454.
[8] (a) R. P. Hausinger, Microbiol. Rev., 1987, 51, 22–42; (b) H. L. Mobley and R. P. Hausinger, Microbiol. Rev., 1989, 53, 85–108; (c) M. J. Maroney and S. Ciurli, Chem. Rev., 2014, 114, 4206–4228; (d) L. Mazzei, F. Musiani and S. Ciurli, J. Biol. Inorg. Chem., 2020, 25, 829–845; (e) L. Mazzei, M. Cianci, S. Benini and S. Ciurli, Angew. Chem., Int. Ed., 2019, 58, 7415–7419.
[9] (a) J. C. Rutherford, PLoS Pathog., 2014, 10, e1004062; (b) B. M. Roesler, E. M. A. Rabelo-Gonçalves and J. M. R. Zeitune, Clin. Med. Insights: Gastroenterol., 2014, 7, 9–17.
[10] I. Konieczna, P. Zarnowiec, M. Kwinkowski, B. Kolesinska, J. Fraczyk, Z. Kaminski and W. Kaca, Curr. Protein Pept. Sci., 2012, 13, 789–806.
[11] (a) B. Marshall and J. R. Warren, Lancet, 1984, 323, 1311–1315; (b) K. A. Eaton, C. L. Brooks, D. R. Morgan and S. Krakowka, Infect. Immun., 1991, 59, 2470–2475; (c) P. Bauerfeind, R. Garner, B. E. Dunn and H. L. T. Mobley, Gut, 1997, 40, 25–30; (d) K. Stingl, K. Altendorf and E. P. Bakker, Trends Microbiol., 2002, 10, 70–74; (e) J. G. Kusters, A. H. van Vliet and E. J. Kuipers, Clin. Microbiol. Rev., 2006, 19, 449–490; (f) J. Baj, A. Forma, M. Sitarz, P. Portincasa, G. Garruti, D. Krasowska and R. Maciejewski, Cells, 2020, 10, 27.
[12] C. Zhou, F. Bhinderwala, M. K. Lehman, V. C. Thomas, S. S. Chaudhari, K. J. Yamada, K. W. Foster, R. Powers, T. Kielian and P. D. Fey, PLoS Pathog., 2019, 15, e1007538.
[13] (a) A. H. Gordon, P. D. Hart and M. R. Young, Nature, 1980, 286, 79–80; (b) D. L. Clemens, B. Y. Lee and M. A. Horwitz, J. Bacteriol., 1995, 177, 5644–5652; (c) W. Lin, V. Mathys, E. L. Y. Ang, V. H. Q. Koh, J. M. Martínez Gómez,M. L. T. Ang, S. Z. Zainul Rahim, M. P. Tan, K. Pethe and S. Alonso, Infect. Immun., 2012, 80, 2771–2779.
[14] R. J. Maier and S. L. Benoit, Inorganics, 2019, 7, 80.
[15] L. Habala, F. Devinsky and A. E. Egger, J. Coord. Chem., 2018, 71, 907–940.
[16] (a) W. Zaborska, B. Krajewska and Z. Olech, J. Enzyme Inhib. Med. Chem., 2004, 19, 65–69; (b) B. Krajewska, J. Enzyme Inhib. Med. Chem., 2008, 23, 535–542; (c) B. Krajewska, J. Mol. Catal. B: Enzym., 2009, 59, 9–21.
[17] (a) L. Mazzei, M. Cianci, A. Gonzalez Vara and S. Ciurli, Dalton Trans., 2018, 47, 8240–8247; (b) L. Mazzei, M. N. Wenzel, M. Cianci, M. Palombo, A. Casini and S. Ciurli, ACS Med. Chem. Lett., 2019, 10, 564–570.
[18] L. Mazzei, M. Cianci, S. Benini, L. Bertini, F. Musiani and S. Ciurli, J. Inorg. Biochem., 2016, 154, 42–49.
[19] S. Benini, C. Gessa and S. Ciurli, Soil Biol. Biochem., 1996, 28, 819–821.
[20] L. Mazzei, D. Cirri, M. Cianci, L. Messori and S. Ciurli, J. Inorg. Biochem., 2021, 218, 111375.

[21] M. Cianci, G. Bourenkov, G. Pompidor, I. Karpics, J. Kallio, I. Bento, M. Roessle, F. Cipriani, S. Fiedler and T. R. Schneider, J. Synchrotron Radiat., 2017, 24, 323–332.
[22] W. Kabsch, Acta Crystallogr., Sect. D: Biol. Crystallogr., 2010, 66, 125–132.
[23] (a) P. Evans, Acta Crystallogr., Sect. D: Biol. Crystallogr., 2006, 62, 72–82; (b) P. R. Evans, Acta Crystallogr., Sect. D: Biol. Crystallogr., 2011, 67, 282–292.
[24] G. N. Murshudov, A. A. Vagin and E. J. Dodson, Acta Crystallogr., Sect. D: Biol. Crystallogr., 1997, 53, 240–255.
[25] L. Mazzei, M. Cianci, U. Contaldo, F. Musiani and S. Ciurli, Biochemistry, 2017, 56, 5391–5404.
[26] E. A. Merritt, Acta Crystallogr., Sect. D: Biol. Crystallogr., 1999, 55, 1109–1117.
[27] (a) P. Emsley and K. Cowtan, Acta Crystallogr., Sect. D: Biol. Crystallogr., 2004, 60, 2126–2132; (b) P. Emsley, B. Lohkamp, W. G. Scott and K. Cowtan, Acta Crystallogr., Sect. D: Biol. Crystallogr., 2010, 66, 486–501.
[28] (a) M. R. Churchill, J. Donahue and F. J. Rotella, Inorg. Chem., 2002, 15, 2752–2758; (b) M. R. Churchill and B. G. DeBoer, Inorg. Chem., 2002, 14, 2502–2507.
399.
[29] E. R. T. Tiekink, Acta Crystallogr., Sect. C: Cryst. Struct. Commun., 1989, 45, 1233–1234.
[30] S. Benini, P. Kosikowska, M. Cianci, L. Mazzei, A. G. Vara, L. Berlicki and S. Ciurli, J. Biol. Inorg. Chem., 2013, 18, 391–399.
[31] L. Mazzei, M. Cianci, S. Benini and S. Ciurli, Chemistry, 2019, 25, 12145–12158.
[32] H. Schmidbaur and A. Schier, Chem. Soc. Rev., 2008, 37, 1931–1951.
[33] L. Casali, L. Mazzei, O. Shemchuk, L. Sharma, K. Honer, F. Grepioni, S. Ciurli, D. Braga and J. Baltrusaitis, ACS Sustainable Chem. Eng., 2019, 7, 2852–2859.
[34] J. Zou, P. Taylor, J. Dornan, S. P. Robinson, M. D. Walkinshaw and P. J. Sadler, Angew. Chem., Int. Ed., 2000, 39, 2931–2934.
[35] H. Sun, Q. Zhang, R. Wang, H. Wang, Y. T. Wong, M.Wang,Q.Hao,A.Yan,R.Y.Kao,P.L.HoandH.Li, Nat. Commun., 2020, 11, 5263.
[36] Z. Adhireksan, G. Palermo, T. Riedel, Z. Ma, R. Muhammad, U. Rothlisberger, P. J. Dyson and C. A. Davey, Nat. Commun., 2017, 8, 14860.
[37] A. Ilari, P. Baiocco, L. Messori, A. Fiorillo, A. Boffi, M. Gramiccia, T. Di Muccio and G. Colotti, Amino Acids, 2012, 42, 803–811.
[38] L. Messori, F. Scaletti, L. Massai, M. A. Cinellu, C. Gabbiani, A. Vergara and A. Merlino, Chem. Commun., 2013, 49, 10100–10102.
[39] D. Parsonage, F. Sheng, K. Hirata, A. Debnath, J. H. McKerrow, S. L. Reed, R. Abagyan, L. B. Poole and L. M. Podust, J. Struct. Biol., 2016, 194, 180–190.
[40] F. Angelucci, A. A. Sayed, D. L. Williams, G. Boumis, M. Brunori, D. Dimastrogiovanni, A. E. Miele, F. Pauly and A. Bellelli, J. Biol. Chem., 2009, 284, 28977–28985.